Ultrasonics 96 (2019) 75–82

Contents lists available at ScienceDirect

Ultrasonics

journal homepage: www.elsevier.com/locate/ultras

Inspection of butt welds for complex surface parts using ultrasonic phased array

Wentao Li[a,*], Zhenggan Zhou[a,b], Yang Li[a]

[a] School of Mechanical Engineering and Automation, Beihang University, Beijing 100083, China
[b] The Collaborative Innovation Center for Advanced Aero-Engine (CICAAE), Beijing 100083, China

ARTICLE INFO

Keywords:
Nondestructive testing (NDT)
Ultrasonic multi-array
Butt weld
Engine blade
Crack defect
Finite element simulation

ABSTRACT

Detection of weld defects for complex surface parts has always been a difficult point in ultrasonic testing because the geometry complexity makes it difficult to arrange transducers and determine the propagation paths of acoustic beams. In this paper, the linear friction weld of the engine blade is taken as an example of the butt weld in complex surface parts, and the application of the ultrasonic array testing method is carried out. Firstly, the propagation properties of acoustic waves in the inspection area are analysed based on both the Snell's law and the acoustic pressure reciprocating transmittance (APRT). According to the inspection requirements, this study establishes a full-coverage inspection solution using multi-array transducers. Secondly, the whole inspection area is divided and the wedge parameters in each subarea are iteratively designed. Thirdly, based on the finite element method (FEM), a response simulation model of the ultrasonic array is established to testify the feasibility and validity of the inspection scheme. Lastly, experiments are conducted on the blade specimen welded by linear friction welding (LFW). The inspection results of different weld positions clearly identify the prefabricated crack defects, showing that the proposed method can fulfill the rapid and accurate inspection for the butt weld of complex surface parts.

1. Introduction

With the development of manufacturing technology, advanced welding technology has been increasingly used in the manufacture of complex surface components. The blisk's blade, a lightweight structure with complex surface, has been widely applied to the new generation of aero engines [1]. Among the existing blisk manufacturing methods, linear friction welding (LFW) is the most important method that first used by Rolls-Royce in 2000 because of its excellent welding quality and high machining efficiency [2]. Meanwhile, due to the complicated welding procedure and the poor work condition, defects in the blade weld often inevitably occur during the processes of manufacturing and the fatigue damage in usage, causing severe security incidents and economic losses [3]. Compared with other kinds of defects, the crack in the weld has a greater impact on the engine blade's performance, and it has a higher probability of occurrence. However, as the butt weld area is located on the root of the blade, it is difficult to achieve this structure's in-service inspection by traditional ultrasonic inspection methods because of the complex surface, the narrow space and the high requirement of inspection precision [4,5]. Accordingly, a new inspection method for the blade welded by LFW has become one of the urgent needs for non-destructive testing (NDT) area to ensure the aeroengine security.

The ultrasonic phased array technique has the characteristics of compact transducer and a high inspection precision because of properly time-delayed pulses of array elements [6]. Therefore, it has some advantages over other non-destructive testing methods for complex structures inspection [7], including turbine rotors [8], corner-shaped components [9] and nuclear power plant components [10]. The research team at the University of Bristol developed an ultrasonic phased array testing system to inspect fir tree roots of turbine blade, whose sensitivity was measured by using an analytical model to predict the propagation of acoustic waves in anisotropic metal alloy materials [11]. Charlesworth designed an integral wedge that could be fully coupled with the roots of the low-pressure turbine rotor blade to meet the in-situ crack inspection requirements in narrow space, and offer higher levels of coverage [12]. Different from the above blade of fir tree tenon/mortise structure, the weld area of the LFW blade to be detected varies greatly in curvature and thickness, which lead to complex ultrasonic propagation path. Therefore, it is of great theoretical and practical significance to develop the ultrasonic phased array inspection method for butt weld of complex surface parts, such as the linear friction weld

* Corresponding author at: Room A108, New Main Building, School of Mechanical Engineering and Automation, Beihang University, Beijing 100083, China.
E-mail address: liwentao@buaa.edu.cn (W. Li).

https://doi.org/10.1016/j.ultras.2019.02.011
Received 14 September 2018; Received in revised form 9 January 2019; Accepted 24 February 2019
Available online 25 February 2019
0041-624X/

on the areoengine blade.

The structural characteristic of the blade's variable curvature and constraints on detection conditions causes the ultrasonic refraction path is very complex and difficult to move the transducer during the detection process. Therefore, it is difficult to obtain defects characteristic information with only one set of ultrasonic array transducer. In addition, it is unrealistic to use the mode of multiple reflection to achieve full coverage of the ultrasonic beam in the detection area because the torsion rate of the component surface is not equal to 0. Therefore, it will be a tedious and time-consuming task to design a set of transducers and wedges at different locations on the blade, at the same time, the accurate blade geometry information is required for design support. In order to design the full coverage inspection scheme of ultrasonic linear multi-array transducer based on the shape information of complex variable curvature structure and iteratively generate the wedge parameters, this paper is composed of the following sections. To begin with, the feasibility of using ultrasonic array method for the inspection of LFW blade is analyzed by combining the ultrasonic theory and the blade's properties. Then, the full-coverage inspection scheme of ultrasonic multi-array transducers is presented, and the parameters of transducers and wedges for each acoustic cross section are designed and optimized using the iterative method. Subsequently, a FEM model is established to analyze the correlation between the inspection parameters and the crack depth. Finally, experiments for the blade specimen of LFW are conducted using 5 MHz, 32 elements linear transducers, and the artificial crack defects (5 mm × 0.2 mm × 0.2 mm) are preformed in a different weld area. The inspection results have proved the validity of the designed ultrasonic phased array method and have shown that this technique effectively improves the efficiency and accuracy of inspection for blades' butt weld in practical applications.

2. Inspection theory

2.1. Propagation of ultrasonic in detection area

In the case of a two-dimensional plane, the propagation of ultrasound between different media follows the Snell's law, as shown in expression:

$$\frac{\sin\alpha}{v_\alpha} = \frac{\sin\beta}{v_\beta} = \frac{\sin\theta}{v_\theta} \tag{1}$$

Here, α, β are the wave angle of incidention and reflection, respectively; θ is refraction angle of longitudinal wave or shear wave; v_α, v_β are the wave velocity of incidention and reflection, respectively; v_θ is the refraction velocity of longitudinal wave or shear wave.

The surface of the blade is a hyperboloid, and the basic theory of wave propagation at the interface between the wedge and the blade is the same as the propagation of the acoustic wave in the ordinary two-dimensional plane, but there are some differences. When the contact surface between two media is a plane, ultrasonic propagation can be equivalent to propagation in the two-dimensional plane because the wave incident point in the wave propagation section and the specimen surface has the same normal vector. However, when the interface between different media is a complex surface, in different sections, the normal vector of the incident point is not necessarily the same on the specimen surface. Here, the condition that the wave in the cross section propagates to the inspection position is the normal vector of the incident wave I, the reflected wave R and the refracted wave T in the same plane, as shown in Fig. 1.

2.2. APRT formulation

The acoustic pressure is usually used to measure the energy of the ultrasonic wave. The inspection results will be more affected by the acoustic transmission energy at the wedge-blade interface when the reflection method is used. The APRT, is defined as the ratio of acoustic pressure of the total reflected wave received by transducer to the acoustic pressure of the incident wave. The factors depend on the angle of incidence, medium density, wave velocities [13].

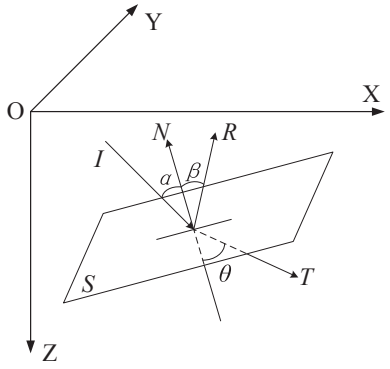

Fig. 1. The schematic diagram of ultrasonic wave propagating to a specified location in a three-dimensional space.

The refracted longitudinal and shear waves may be generated from an oblique incident wave at a solid-solid interface, depending on the wave velocities in the two media and the incidence angle [14]. The acoustic pressure transmission coefficient (APTC) of refracted longitudinal wave can be written as follows for longitudinal wave input:

$$T_{LL} = \frac{2\rho_2 c_{L2} c_{T2}^2 c_{L1} \cos^2 2\beta_{T2} \cos 2\alpha_{L1}}{N\rho_1 c_{T1}^4 \cos 2\alpha_{L1} \sin\alpha_{L1}} \tag{2}$$

$$N = 2\cot\alpha_{T1} + \frac{c_{L1}}{2c_{T1}} \cdot \frac{\cos^2 2\alpha_{T1}}{\cos\alpha_{L1}} + \frac{2\rho_2 c_{T2}^4}{\rho_1 c_{T1}^4}\cot\beta_{T2} + \frac{\rho_2 c_{L1} c_{T2}^2}{2\rho_1 c_{T1}^4} \cdot \frac{\cos^2 2\beta_{T2}}{\cos\alpha_{L1}} \tag{3}$$

Here, ρ_1, c_{L1} and c_{T1} are density, longitudinal and transverse wave velocities in medium-1; ρ_2, c_{L2} and c_{T2} are density, longitudinal and transverse wave velocities in medium-2, respectively. The incident or reflection in medium-1 angle is either α_{L1} for a longitudinal wave or α_{T1} for a transverse (shear) wave; β_{T2} is refraction angle of transverse wave in medium-2. For a refraction transverse wave, the APTC can be expressed as:

$$T_{TL} = \frac{-2\rho_2 c_{T2}^3 c_{L1} \cos 2\alpha_{T1}}{N\rho_1 c_{T1}^4 \sin 2\alpha_{L1}} \tag{4}$$

For transverse wave input, the APTC for refraction longitudinal wave and transverse wave can be written as follows:

$$T_{LT} = \frac{-4\rho_2 c_{L2} c_{T2}^2 c_{L1} \cos^2 2\beta_{T2} \cos 2\alpha_{T1}}{N\rho_1 c_{T1}^4 \sin\alpha_{L1}} \tag{5}$$

$$T_{TT} = \frac{4\rho_2 c_{T2}^3 c_{L1} \cos\alpha_{T1}}{N\rho_1 c_{T1}^4 \sin\alpha_{L1}} \tag{6}$$

The APTC of ultrasonic waves returned from medium-2 to medium-1 can be obtained by changing the corresponding media parameters derived from Eqs. (2)–(6). The APRT in this case is defined as:

$$T_R = T_{12} \cdot T_{21} \tag{7}$$

where T_{12} is the APTC for medium-1 to medium-2, but change to T_{21} is the APTC for medium-2 to medium-1.

The material for the wedge is rexolite, and the properties of wedge and specimen are shown in Table 1. The refracted longitudinal and transverse waves are generated in the blade because of the wave mode-conversion caused by oblique incidence of longitudinal wave at the wedge-blade interface. The APRT of the longitudinal and transverse waves for longitudinal wave input method are changed with the incident angle. Fig. 2 shows the APRT of longitudinal and transverse

Table 1
Wedge and specimen properties.

Property	Wedge	Specimen
Density (kg/m^3)	1050	4540
L-wave velocity (m/s)	2337	6008
S-wave velocity (m/s)	1155	2958
Modulus of elasticity (Gape)	4.0077	106.4
Poisson ratio	0.32	0.34

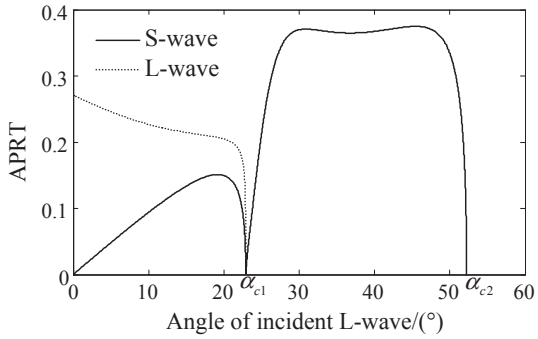

Fig. 2. The APRT of longitudinal and transverse waves from wedge into the blade that oblique incident angles from 0° to 90°.

waves from wedge into the blade that oblique incident angles from 0° to 90°. In the Fig. 2, α_{c1} and α_{c2} are the first and second critical angles of rexolite to titanium alloy, respectively.

3. Design of inspection scheme

3.1. Area division and information extraction for blade

The weld joint runs through the entire blade, and has the length of about 160 mm. There are different curvature and thickness variations at different positions of weld, so parameter extraction is a necessary prerequisite for designing an ultrasonic array inspection scheme. Assuming *N*-group transducers are to be designed, it is necessary to divide *N* sub-regions accurately and extract *N*-group 2D cross-section NURBS (Non-uniform rational basis spline) curves on the CAD model. Although it is unreasonable to design the beam main plane and propagation path of a variable curvature component by using a 2D profile, this problem is considered in the subsequent design iteration method and a successive approximation iteration method is used to determine the beam main plane. The inspection area is divided into twenty different subareas according to the degree of curvature change to meet the full coverage inspection requirements for the weld area, using the linear transducers. Each inspected area along the blade width direction is about 6–10 mm (about 1/20 of the whole blade width) according to the degree of curvature change. As shown in Fig. 3, which simplifies the complexity of the incident wave calculation and the wedge parameters design with ignoring the effect of curvature changes for each subarea.

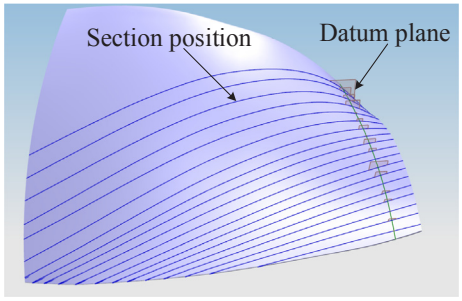

Fig. 3. Division for the weld area according to the degree of curvature change.

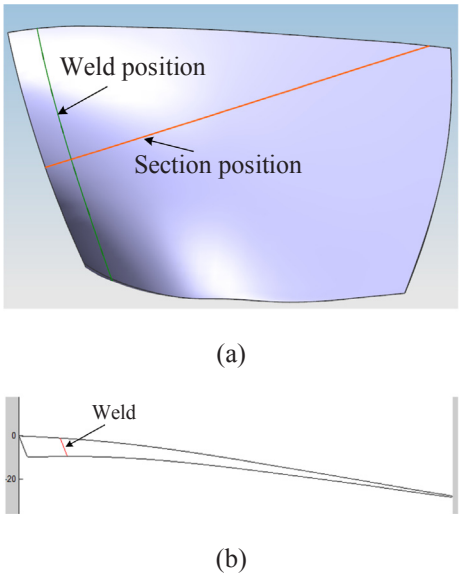

Fig. 4. Geometry information extraction of a section from CAD model of the blade (a), and (b) shows the section reconstruction result.

As shown in Fig. 4(a), in order to obtain the accurate geometric shape information of a measured cross section, the geometrical parameters of the CAD model include the information of the surface equation, the normal vectors and the curvature radius are extracted and analyzed by UGNX API. The extracted information combined with the NURBS method to reconstruct and characterize the ray tracing module, as shown in Fig. 4(b).

3.2. Iterative design of wedge parameters

The defects in weld area cannot be detected by conventional multiple reflections at an inspection position due to the curved surface structure of the blade. Therefore, the weld near the lower surface at each inspection position is inspected using a probe placed on the upper surface of the blade, and the weld near the upper surface is inspected by a probe placed on the lower surface of the blade to achieve full coverage inspection of the weld area, as shown in Fig. 5(a) and (b). Thus, it is need to design two wedges for each inspection position, which means that 38 wedges should be designed for the 19 positions of the blade. In addition, a single component wave should be guaranteed into the blade for obtain high detection precision and high reliability. In this paper, the inclination angle of the wedge is designed for each inspection position and an iterative design and optimization method is established to improve efficiency.

The wedge design and optimization process of the inspection scheme are introduced based on an original central section-A for the inspection position. Firstly, as shown in Fig. 6(a), the appropriate incident point *O* is determined by the mode-conversion conditions of refracted beam *OF* and the distance of incident waves. However, the section normal vector *N1* and the surface normal vector *N2* at the point *O* are likely to be different, so the main acoustic beam cannot propagate to the point *F* from the cross section-A in the three-dimensional space. Accordingly, we need to perform a cross-multiplication operation to determine a new cross section-A′ based on the refractive line *OF* and its normal vector *N2* at the intersection of the blade surfaces. This process is combined with the secondary development function of UG again, and the cross-multiplication operation is converted into the reference plane construction which is used to intersect with the blade model to obtain a new cross section.

Then, the NURBS curve information of the new section is extracted again for wedge design. The design procedures and criteria of the main

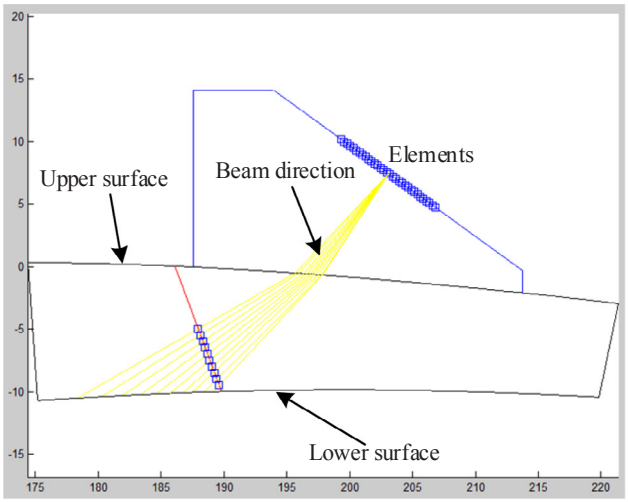

Fig. 5. Schematic diagram of the full coverage inspection for the weld (a) Inspection for lower part weld (b) Inspection for upper part weld.

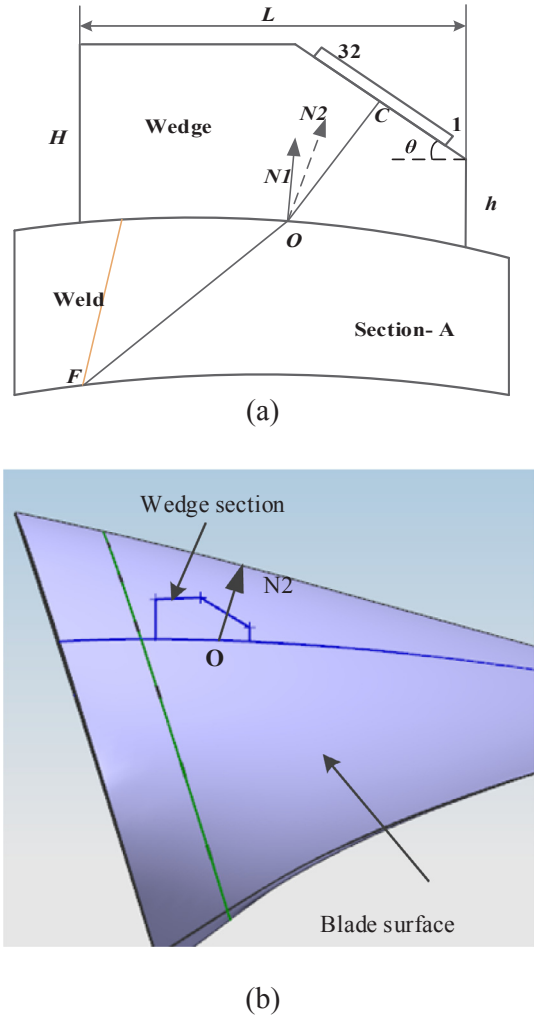

Fig. 6. Diagram of wedge design procedure (a) Wave propagation in the section-A (b) Establishment of the wedge parameters on the section-A.

wedge parameters are set as follows: the equivalent incident beam *CO* at the incident point *O* is calculated using the equivalent refraction beam *OF* and the new section normal vector *N2* according to Fermat's principle. Point *C* is the center of the transducer, and the inclination direction of the wedge is along the vertical direction of the *CO*. The length *L* of the wedge is determined according to the transducer size and the beam propagation path of starting element and termination element. In addition, due to the narrow inspection space so that the height *H* does not exceed 30 mm by adjusting the length of *CO*, while the thinnest wedge thickness *h* is not less than 3 mm to meet the processing requirements. Fig. 6(b) shows the wedge parameters of section-A obtained from the above design flow.

On this basis, the inclination angle of the wedge should be redesigned because the main plane (central section) of the wedge has been changed. According to the APRT change rule of longitudinal wave from the wedge to the blade, the incident angle $\theta_i (1 \leqslant i \leqslant 32)$ of each element should satisfy the following relation:

$$\alpha_{C1} < \theta_i < \alpha_{C2} \tag{8}$$

The Fig. 2 shows that the APRT of transverse wave is higher when the incident angle is between 29° and 47° so that the incidence angles θ_i of all the elements best within the range of [29°, 47°]. Due to the large number of wedges need to be designed, in order to improve the design efficiency, an iterative design process is established based on the design criteria mentioned above.

Based on these results, it is judged whether the incidence angle of all array elements in the section-A′ is within the optimal range. Otherwise, on the basis of the design results, the initial intersection point *O* is moved back or forth, and the whole process is iterated repeatedly until the optimal parameters are reached. At this point, only the 2D cross section of the wedge is obtained based on the above design process. Therefore, according to the curvature at the location of the wedge, 3–5 mm is drawn to both sides of the cross section to obtain all the final parameters of the wedge. The design of the full coverage inspection scheme for the weld area is accomplished by designing and optimizing the wedges of the all 38 sections, and the location of the transducers and the wedges are shown in Fig. 7(a) and (b). In order to avoid the formation of a blind zone between the two transducers, the beam main plane is established by taking the junction position of each transducer as a new division position. According to the above method, two sets of supplementary transducers can be designed to ensure the overlap of beam coverage and avoid missed detection.

3.3. Finite element simulation

In order to verify the correctness of the wedge parameters and the main section, the simulation model of the blade and wedge is

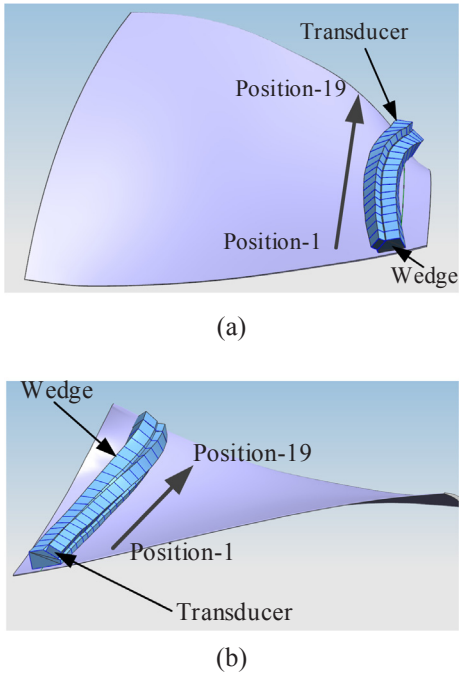

Fig. 7. The overall design result of the Wedge's parameters on the blade surface (a) The upper surface (b) The lower surface.

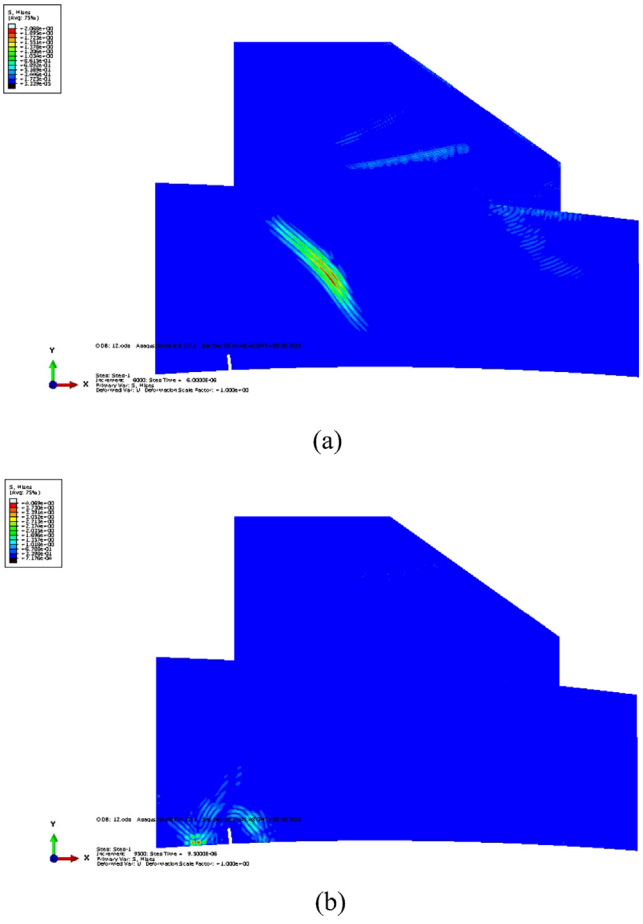

Fig. 8. (a) and (b) show the propagation of the array synthetic beam in simulation model at 6 μs and 10 μs, respectively.

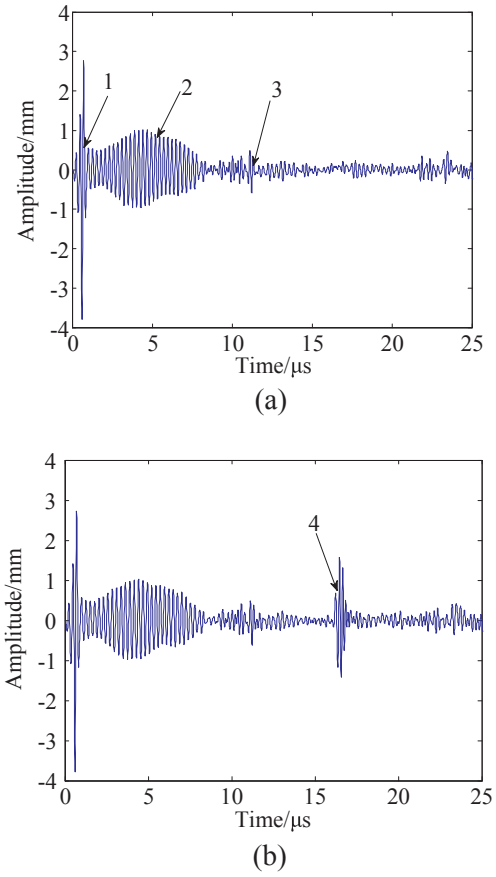

Fig. 9. A-scan view of simulated results (a) without defect (b) with defect.

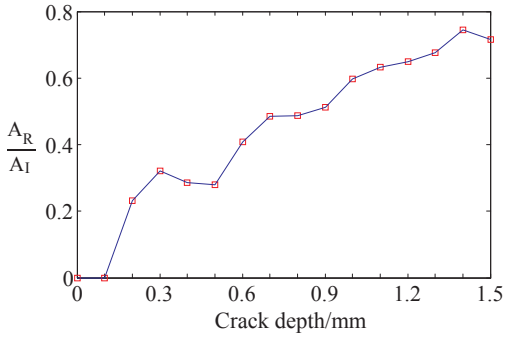

Fig. 10. The simulation result of different crack depths on inspectability.

established on the Abaqus platform according to the inspection scheme and the parameters in Table 1. The Abaqus script code based on the combination of MATLAB and Python realizes the automation of defining wedge, meshing, loading excitation delay scheme and so on. Only the section near the weld area is calculated to improve the calculation efficiency because of the larger cross section of the blade profile, and the absorption layer of the incident wave is set at the truncated boundary [15,16].

The simulation calculation is based on the Abaqus/Explicit analysis module, which applies the pressure load perpendicularly to 32 linear nodes with a pitch of 0.4 mm and width of 0.3 mm on the wedge surface to simulate element parameters. Additionally, a three-circle, Gaussian window pulse with a center frequency 5 MHz is used as the excitation signal to simulate the transducer with 5 MHz center frequency and 32 elements. The bottom of the blade weld has a groove with the depth of 0.6 mm and the width of 0.2 mm to simulate the crack defect. The phase delay of the modulation signal of each node is made based on the delay

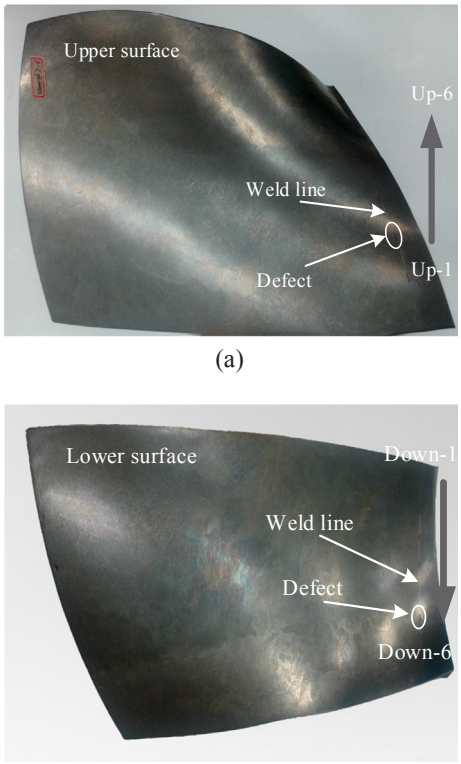

Fig. 11. The blade specimen with 12 prefabricated defects on the butt weld. (a) Defects and identifiers on upper blade surface. (b) Defects and identifiers on lower blade surface.

focusing law so that the ultrasonic wave is focused on the crack. Due to the complex geometric structure, the model is scaled by a three-node linear unit of CPE3 type with a grid size of 0.02 mm. Besides, the time step size is set to be 1 ns and the total computation time is 25 μs. Fig. 8 shows the simulation model of ultrasonic propagation in the wedge and blade.

Fig. 9 shows the simulated A-scan images in defective and defect-free cases that the amplitude is synthesized by the phase delay of the X and Y displacement components of the 32 nodes. In Fig. 9(a), the 1 is the initial wave, and the 2 is the clutter caused by mutual interference between the elements, the 3 is the reflected echo of the wedge-blade interface, and the 4 in Fig. 9(b) is the defect echo.

There are 15 different cracks depth are simulated from 0.1 mm to 1.5 mm at 0.1 mm intervals to analyze the effect of crack depth on inspectability. Fig. 10 shows the simulation result of different crack depths on inspectability. The abscissa is the depth of the crack, and the ordinate represents the amplitude ratio of the crack echo to the initial wave, in which A_R is the defect echo peak and A_I is the initial wave peak. In general, the inspectability increases with the increasing of the crack depth. At this position, the crack with depth of 0.2 mm and above can be detected, the crack depth of 0.1 mm is not recognized. All the 38 wedge positions in the scheme are validated and analyzed by the finite element simulation model, respectively, since the crack angle and the relative position of the weld are different for each transducer and wedge. The simulation results show that the design parameters and the delay time calculation method in the inspection scheme can realize the crack defects inspection of not less than 0.2 mm depth at different inspection positions of the blade.

4. Experimental validation

The specimen is an integral blade that has been welded with the root using LFW and contains a butt weld, as shown in Fig. 11. Six rectangular artificial defects (5.0 mm × 0.2 mm × 0.2 mm groove) were machined at different curvatures of the weld position on the upper and lower surfaces, respectively, which the length direction is the same as the extension direction of the weld. Each artificial defects are numbered in order to facilitate the expression of the inspection process and

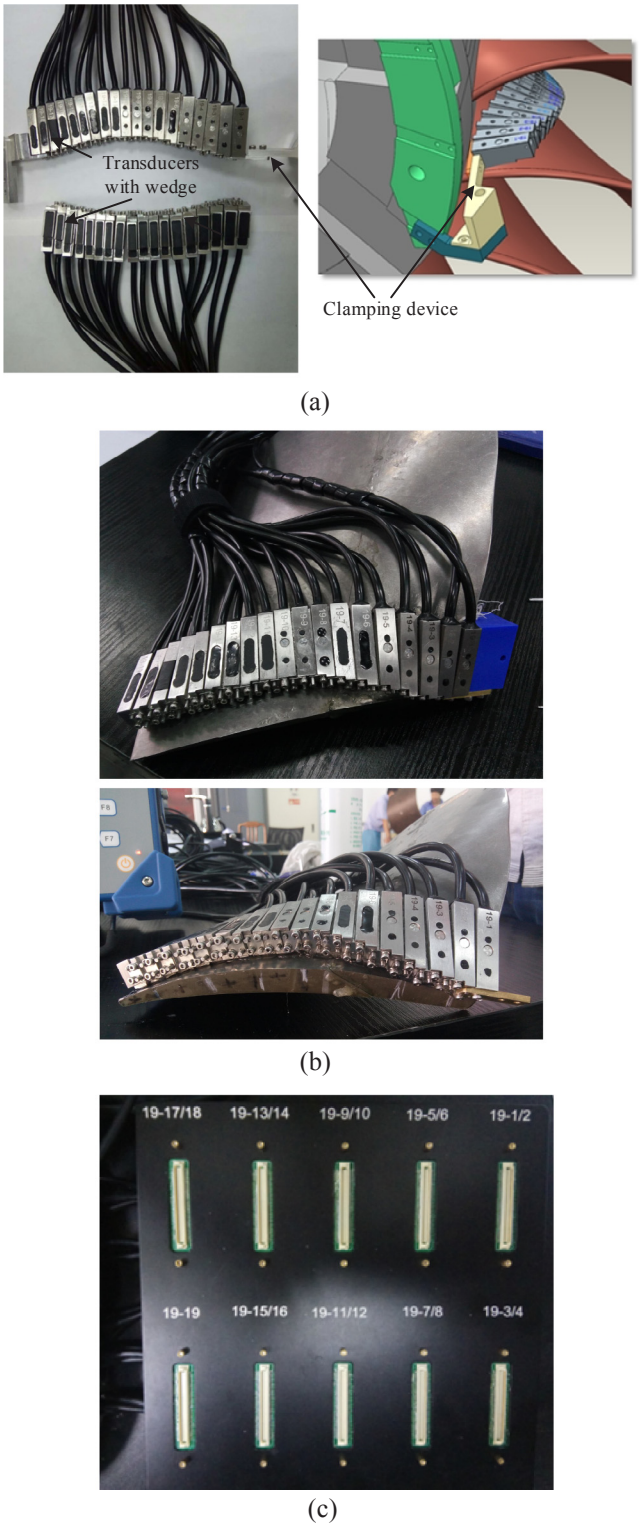

Fig. 12. (a) The transducers and clamping device. (b) Manual coupling for experiments. (c) A dedicated commutator used to switch the working state of different transducers.

Table 2
Experiment parameters.

Frequency	Elements number	Apertures
5 MHz	32	32
Scanning angle	Focus depth	Scan type
40–70°	10–20 mm	S-scan

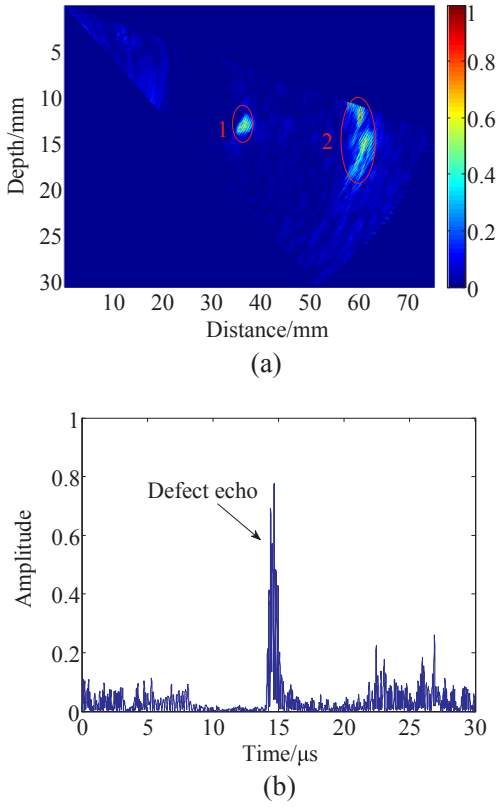

Fig. 13. Experimental images for the Up-3 defect. (a) S-scan view. (b) A-scan view.

results. As arrow direction shown in Fig. 11(a), the artificial defects on the upper surface is sequentially numbered as Up-1, Up-2, Up-3, Up-4, Up-5 and Up-6. Similarly, the lower surface defects are numbered Down-1 to Down-6 in the arrow direction in Fig. 11(b).

In general, the transducer and the wedge are two separate parts. In this project, an integrated transducers and wedges are designed and manufactured to reduce the overall size due to the small inspection space in field detection. The transducer arrays and connection device for the upper and lower surfaces are shown in Fig. 12(a). In the actual inspection process, the transducers are fixed to the designed inspection position of the blade by a clamping device. Manual fitting is used in this experiment because of the separated blade specimen, and the operating status of each transducers are controlled by the dedicated commutator, as shown in Fig. 12(b) and (c) respectively. The main inspection parameters for blade specimen are given in Table 2.

Through the above inspection scheme and process, the inspection for the all blade weld area was realized in a short time, and the twelve artificial defects were successfully inspected. In this paper, three inspection results of typical defect- prefabricated positions are selected to illustrate in Figs. 13–15, respectively. In the figure, the 1 is the defect echo, and the 2 is the boundary echo caused by the interface of the blead specimen root. Fig. 13(a) shows the S-scan image of the Up-3 defect at the middle weld area where the curvature change is relatively small. The A-scan image of an angle from Fig. 13(a) is shown in Fig. 13(b), from which the defect can be determined clearly. The images

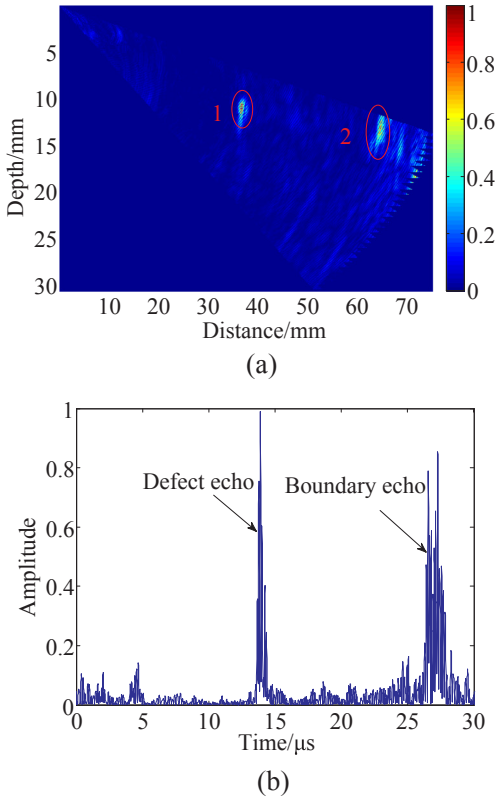

Fig. 14. Experimental images for the Down-1 defect. (a) S-scan view. (b) A-scan view.

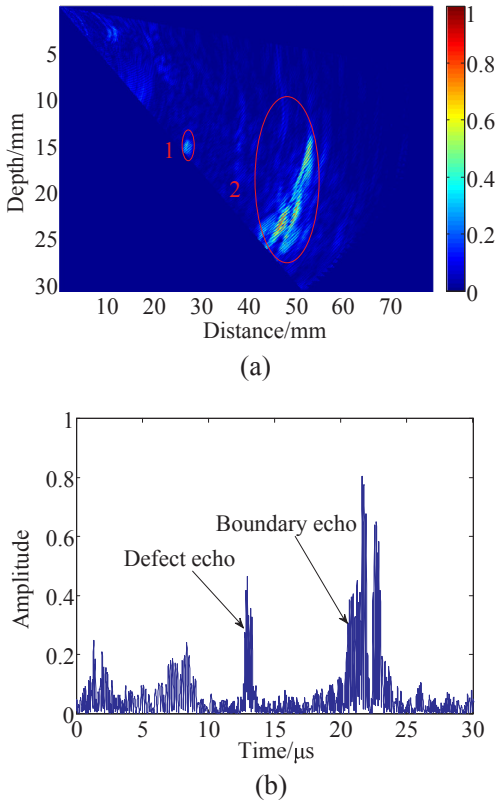

Fig. 15. Experimental images for the Down-5 defect. (a) S-scan view. (b) A-scan view.

in Figs. 14 and 15 are the Down-1 and Dowm-5 defect inspection results of the weld area which near the blade boundary with large curvature change, and the good experiment results can also be seen from the A-scan and the S-scan images.

5. Summary and conclusions

The full-coverage inspection scheme is presented based on ultrasonic phased array technique to meet the fast and accurate inspection requirements of butt weld for the aeraengine blade. The ultrasonic theory in complex interface of wedge and blade is analyzed as well. The appropriate transducers and wedges are designed, which can be applied to inspection scheme design for complex surface parts.

The propagation properties of ultrasonic wave based on Snell's law in the complex curved surface for the blade and the APRT of wedge-blade interface at different incident angles are discussed. It is proved that when the deflection angle of incident beam ranges from 29 to 47 degrees, there is strong acoustic transmission energy inside the weld area. Based on the research mentioned above, the wedge parameters for each divided inspection area are iterative designed to realize the accurate beam control and improved design efficiency. The ultrasonic phased array model based on FEM for the engine blade is established and the ultrasonic loading scheme is designed according to the calculation principle of the focusing law. It show that the FEM is an effective tool in researching ultrasonic inspection analysis with complex surface. And further, the inspectability of the crack depth at each transducer position is simulated and analyzed. In the simulation results, the defect echo signal of crack depth greater than 0.2 mm can be clearly distinguished with high SNR that verified the feasibility and effectiveness of the proposed scheme in theory.

Finally, the ultrasonic inspection experiment of the blade specimen with artificial crack defects of 0.2 mm depth was conducted using integrated transducers with 32 elements and 5 MHz center frequency. The inspection results show that the design scheme have a good application on crack inspection of linear friction weld. The proposed scheme of ultrasonic array has been successfully applied to the field detection of the engine blade welded by LFW and has good application prospects in other butt weld of complex surface components.

Acknowledgements

This work is supported by National Natural Science Foundation of China (NSFC) No. 51775026.

Appendix A. Supplementary material

Supplementary data to this article can be found online at https://doi.org/10.1016/j.ultras.2019.02.011.

References

[1] B.V.R. Ravi-Kumar, A review on BLISK technology, Int. J. Innovat. Res. Sci., Eng. Technol. 2 (5) (2013) 1353–1358.
[2] A.M.M. García, BLISK Fabrication by Linear Friction Welding, In Tech, Rijeka, 2010 https://doi.org/10.5772/21278.
[3] A. Morita, H. Kagawa, M. Sugawara, et al., Evaluation of corrosion fatigue crack propagation life at low-pressure steam turbine rotor groove, Eng. Fract. Mech. 73 (12) (2006) 1615–1628.
[4] Z.L. Bai, S.L. Chen, L.C. Jia, et al., Phased array ultrasonic signal compressive detection in low-pressure turbine disc, NDT and E Int. 89 (2017) 1–13.
[5] S. Yang, B. Yoon, Y. Kim, Using phased array ultrasonic technique for the inspection of straddle mount-type low-pressure turbine disc, NDT and E Int. 42 (2) (2009) 128–132.
[6] Z. Jie, W.D. Bruce, D.W. Paul, et al., Defect detection using ultrasonic arrays: The multi-mode total focusing method, NDT and E Int. 43 (2) (2010) 123–133.
[7] B.W. Drinkwater, P.D. Wilcox, Ultrasonic arrays for nondestructive evaluation: a review, NDT and E Int. 39 (7) (2006) 525–541.
[8] X. Guan, J. Zhang, E.M. Rasselkorde, et al., Material damage diagnosis and characterization for turbine rotors using three-dimensional adaptive ultrasonic NDE data reconstruction techniques, Ultrasonics 54 (2014) 516–525.
[9] N. Xu, Z.G. Zhou, Numerical simulation and experiment for inspection of corner-shaped components using ultrasonic phased array, NDT and E Int. 63 (2014) 28–34.
[10] S.J. Song, H.J. Shin, Y.H. Jang, Development of an ultrasonic phased array system for non-destructive tests of nuclear power plant components, Nucl. Eng. Des. 214 (2002) 151–161.
[11] L. Christopher, The Development of a 2D Ultrasonic Array Inspection for Single Crystal Turbine Blades, University of Bristol, British, 2011.
[12] C. Charlesworth, Phased array ultrasonic inspection of low-pressure steam turbine rotors - curved axial entry fir tree roots, INSIGHT 53 (2) (2011) 71–75.
[13] L.R. Joseph, Ultrasonic Waves in Solid Media, Cambridge University Press, Cambridge, 2000, pp. 55–63.
[14] W. Lester, J.R. Schmerr, Fundamentals of Ultrasonic Phased Arrays, Springer International Press, Iowa State University, 2015, pp. 38–42.
[15] M. Castaings, C. Bacon, Finite Element modeling of torsional wave modes along pipes with absorbing materials, J. Acoust. Soc. Am. 119 (6) (2006) 3741–3751.
[16] Z. Peng, Y. Xudong, F. Zheng, Numerical modeling of embedded solid waveguides using SAFE-PML approach using a commercially available finite element package, NDT and E Int. 90 (2017) 11–23.